

Using cylindrical algebraic decomposition and local Fourier analysis to study numerical methods: two examples

Stefan Takacs

Faculty for Mathematics,

Research Group Numerical Mathematics (Partial Differential Equations),

TU Chemnitz, Germany

Email: stefan.takacs@numa.uni-linz.ac.at

Abstract—Local Fourier analysis is a strong and well-established tool for analyzing the convergence of numerical methods for partial differential equations. The key idea of local Fourier analysis is to represent the occurring functions in terms of a Fourier series and to use this representation to study certain properties of the particular numerical method, like the convergence rate or an error estimate.

In the process of applying a local Fourier analysis, it is typically necessary to determine the supremum of a more or less complicated term with respect to all frequencies and, potentially, other variables. The problem of computing such a supremum can be rewritten as a quantifier elimination problem, which can be solved with cylindrical algebraic decomposition, a well-known tool from symbolic computation.

The combination of local Fourier analysis and cylindrical algebraic decomposition is a machinery that can be applied to a wide class of problems. In the present paper, we will discuss two examples. The first example is to compute the convergence rate of a multigrid method. As second example we will see that the machinery can also be used to do something rather different: We will compare approximation error estimates for different kinds of discretizations.

Index Terms—Multigrid; Fourier analysis; Cylindrical algebraic decomposition

I. INTRODUCTION

In this paper, we want to give some examples where the combination of cylindrical algebraic decomposition (CAD), as a tool from symbolic computation, and local Fourier analysis (LFA) yield helpful results. LFA was introduced by A. Brandt, who proposed to use Fourier series to analyze multigrid methods, cf. [1]. For a detailed introduction into LFA, see, e.g., [10]. LFA provides a framework to determine sharp bounds for the convergence rates of multigrid methods and other iterative solvers for problems arising from partial differential equations. This is different to classical analysis, which typically yields qualitative statements only. So classical convergence proofs for multigrid solvers, cf. [5], show that the method is convergent and that the convergence rates are uniformly bounded away from 1 for all grid sizes, however there is no sharp, nor realistic bound for the convergence rate given. Besides the analysis of linear solvers, the idea of LFA can be carried over to other applications, like the computation

of approximation error estimates or the computation of inverse inequalities.

LFA can be justified rigorously only in special cases, e.g., on rectangular domains with uniform grids and periodic boundary conditions. However, results obtained with LFA can be carried over to more general cases, see, e.g. [2]. In cases, where such an extension is not possible, it can be seen as heuristic approach.

To compute the quantities of interest using LFA, typically one has to compute the supremum of a more or less complicated term. The key for involving symbolic algorithms is a proper reformulation of the problem of computing a supremum as a quantifier elimination problem, which can be solved using a CAD algorithm, cf. [4]. Understanding the combination of LFA and CAD as a machinery for analyzing a numerical method, we apply this machinery in the present paper to two examples, keeping in mind that there are more.

The first example is related to the classical idea of analyzing multigrid solvers. In Sec. II, we will introduce a classical finite element framework for the Laplace equation and analyze a standard Jacobi iteration for solving the discretized system. There, we will introduce the reader to the finite element method to keep the paper readable also for non-numerical analysts. In Sec. III, we will extend the analysis to be able to learn about convergence properties of a multigrid solver. The given example is rather simple (and could be solved also without use of CAD, just per hand). However, we refer to other examples, where the terms get much more complicated, which make symbolic tools more interesting, cf., e.g., [7] and [8].

The second example, which will be discussed in Sec. IV, is a new result. It is given to show that the machinery of LFA can also be extended to analysis beyond analyzing the convergence of a multigrid solver. We will see that the method can also be used to develop approximation error estimates. Moreover, we will see that LFA can capture any kind of discretization. To keep it simple, we will stay in the one dimensional case, so the terms, that have to be resolved using CAD, are rather easy. We will provide supplementary material that covers also the extension to two dimensions. There, one can see that in this case the terms get much more complicated.

This list of examples is not complete. So, CAD has already

been applied earlier in the analysis of (systems of) ordinary and partial differential-difference equations, [6], where the necessary conditions for stability, asymptotic stability and well-posedness of the given systems were transformed into statements on polynomial inequalities using Fourier or Laplace transforms.

II. FINITE ELEMENT METHOD AND A SIMPLE ITERATION SCHEME

We start our analysis with a simple example, the Laplace equation. For a given function f , we are interested in finding a function u such that

$$-u''(x) = f(x) \quad (1)$$

is satisfied for all $x \in \Omega := (0, 1)$ and, moreover, the boundary condition $u(0) = u(1) = 0$ holds.

The standard way of solving this, is to introduce a variational formulation. Let $H^1(\Omega)$ be the standard Sobolev space of weakly differentiable functions and $H_0^1(\Omega) \subset H^1(\Omega)$ be the space of functions that moreover satisfy the boundary condition $u(0) = u(1) = 0$. Then, the strong formulation (1) can be rewritten in weak formulation as follows: Find $u \in V := H_0^1(\Omega)$ such that

$$\int_{\Omega} u'(x)v'(x)dx = \int_{\Omega} f(x)v(x)dx \quad (2)$$

for all $v \in V$, cf. standard literature on finite elements, like [3].

For any finite dimensional subset $V_k \subset V$, we can introduce a discretized problem: Find $u_k \in V_k$ such that

$$\int_{\Omega} u_k'(x)v_k'(x)dx = \int_{\Omega} f(x)v_k(x)dx \quad (3)$$

for all $v_k \in V_k$. The approach to use the same space, V_k , for both, u_k and v_k , is called the Galerkin principle. This guarantees that u_k is the orthogonal projection of the exact solution $u \in V$ into V_k .

The easiest way to set up the space V_k is to choose the Courant element: Here the domain Ω is subdivided into intervals (in one dimension) or into triangles (in two dimensions). We call these intervals or triangles *elements*. The space V_k consists of all globally continuous functions that are linear on each element.

Each function in V_k can be characterized just by prescribing its values on the end points of the intervals or at the vertices of the triangles, respectively – we call these points *nodes*. This fact can be used to construct a basis: The nodal basis of V_k is the collection of all functions $\varphi_{k,i} \in V_k$ that take the value 1 on exactly one of the nodes and the value 0 on all of the other nodes. One such basis function is visualized in Fig. 1.

Having this basis, we can represent the functions u_k and v_k in terms of the basis:

$$u_k(x) = \sum_{i=1}^N u_{k,i} \varphi_{k,i}(x), \quad v_k(x) = \sum_{i=1}^N v_{k,i} \varphi_{k,i}(x),$$

where the functions u_k and v_k can be represented by the coefficient vectors $\underline{u}_k := (u_{k,i})_{i=1}^N$ and $\underline{v}_k := (v_{k,i})_{i=1}^N$.

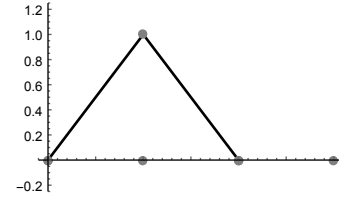


Fig. 1. Basis functions of standard Courant element

The variational equality (3) can be rewritten in matrix-vector notation as follows:

$$\underline{v}_k^T K_k \underline{u}_k = \underline{v}_k^T \underline{f}_k, \quad (4)$$

for all $\underline{v}_k \in \mathbb{R}^N$, where $K_k := (\int_{\Omega} \varphi'_{k,j}(x)\varphi'_{k,i}(x)dx)_{i,j=1}^N$ and $\underline{f}_k := (\int_{\Omega} f_k(x)\varphi_{k,i}(x)dx)_{i=1}^N$. As (4) is supposed to be satisfied for all \underline{v}_k , it can be rewritten as follows: Find \underline{u}_k such that

$$K_k \underline{u}_k = \underline{f}_k. \quad (5)$$

To obtain a good approximation, it is often necessary to refine the intervals (or triangles) used for the discretization of the partial differential equation. In this case both, the number of unknowns and the condition number of the matrix K_k , grow. However, K_k has a nice property: it symmetric and positive definite.

A simple linear iteration scheme to solve a matrix-vector problem (5) for K_k being symmetric and positive definite, is the (damped) Jacobi iteration. Assuming $\underline{u}_k^{(0)}$ to be some starting value, the iteration procedure is given by

$$\underline{u}_k^{(m+1)} := \underline{u}_k^{(m)} + \tau(\text{diag} K_k)^{-1}(\underline{f}_k - K_k \underline{u}_k^{(m)}),$$

where $\tau > 0$ is a given damping parameter. For $\tau = 1$, we obtain the standard Jacobi iteration.

As a next step, we are interesting in analyzing the convergence of the Jacobi iteration scheme. So, using the exact solution $\underline{u}_k^* := K_k^{-1} \underline{f}_k$, we obtain

$$\underline{u}_k^{(m+1)} - \underline{u}_k^* = (I - \tau(\text{diag} K_k)^{-1} K_k)(\underline{u}_k^{(m)} - \underline{u}_k^*)$$

and further

$$\|\underline{u}_k^{(m+1)} - \underline{u}_k^*\|_{K_k} \leq \|I - \tau(\text{diag} K_k)^{-1} K_k\|_{K_k} \|\underline{u}_k^{(m)} - \underline{u}_k^*\|_{K_k},$$

where $\mathcal{S}_k := I - \tau(\text{diag} K_k)^{-1} K_k$ is called the iteration matrix and $\|\cdot\|_{K_k}$ is the vector norm $\|\underline{v}_k\|_{K_k} := (\underline{v}_k^T K_k \underline{v}_k)^{1/2}$ or the associated matrix norm. We have

$$\|\mathcal{S}_k\|_{K_k} = \|K_k^{1/2}(I - \tau(\text{diag} K_k)^{-1} K_k)K_k^{-1/2}\|,$$

where $\|\cdot\|$ is the standard Euclidean norm. As $K_k^{1/2}(I - \tau(\text{diag} K_k)^{-1} K_k)K_k^{-1/2}$ is symmetric, obtain further

$$\|\mathcal{S}_k\|_{K_k} = \rho(K_k^{1/2}(I - \tau(\text{diag} K_k)^{-1} K_k)K_k^{-1/2}) = \rho(\mathcal{S}_k),$$

where $\rho(\cdot)$ is the spectral radius.

To determine the spectral radius, we use LFA: We compute the spectral radius of \mathcal{S}_k explicitly for a special case. We assume to have

- an infinitely large domain Ω (this neglects all influence coming from the boundary of the domain),

which is

- discretized using an uniform (equidistant) grid.

For simplicity, here, we restrict ourselves to the one dimensional case. However, LFA can also be worked out for two or more dimensions, cf. [10].

For such an equidistant grid, we can compute the stiffness matrix K_k explicitly:

$$K_k = \frac{1}{h_k} \begin{pmatrix} \ddots & \ddots & & & & & \\ & 2 & -1 & & & & \\ & -1 & 2 & -1 & & & \\ & & -1 & 2 & -1 & & \\ & & & -1 & 2 & \ddots & \\ & & & & & \ddots & \ddots \end{pmatrix},$$

where h_k is the grid size (length of the intervals).

As next step, we define for any frequency $\theta \in [0, 2\pi)^d$ a vector of complex exponentials

$$\underline{\phi}_k(\theta) := (\phi_{k,j}(\theta))_{j \in \mathbb{Z}} := (e^{j\theta i})_{j \in \mathbb{Z}}$$

and observe that

$$K_k \underline{\phi}_k(\theta) = \underbrace{\frac{1}{h_k} (-e^{-\theta i} + 2 - e^{\theta i})}_{\widehat{K}_k(\theta)} \underline{\phi}_k(\theta) \quad (6)$$

is satisfied, i.e., that $\underline{\phi}_k(\theta)$ is an eigenvector of K_k . In the LFA world, the eigenvalue $\widehat{K}_k(\theta)$ is also called the symbol of K_k .

Based on the symbol of K_k , we can determine the symbol (eigenvalue) of the iteration matrix \mathcal{S}_k . First note that $\text{diag} K_k = \frac{2}{h_k} I$ and therefore $\text{diag} \widehat{K}_k(\theta) = \frac{2}{h_k}$. So, we obtain

$$\begin{aligned} \widehat{\mathcal{S}}_k(\theta) &= 1 - \tau \frac{h_k}{2} \widehat{K}_k(\theta) \\ &= 1 - \frac{\tau}{2} (-e^{-\theta i} + 2 - e^{\theta i}) = 1 - \tau(1 - \cos \theta). \end{aligned} \quad (7)$$

As we have mentioned above, we are interested in $\rho(\mathcal{S}_k)$. This spectral radius can be expressed using the symbol:

$$q(\tau) := \rho(\mathcal{S}_k) = \sup_{\theta \in [0, 2\pi)} |\widehat{\mathcal{S}}_k(\theta)| = \sup_{\theta \in [0, 2\pi)} |1 - \tau(1 - \cos \theta)|.$$

By substituting the variable θ by $c := \cos \theta$, we can completely eliminate the occurrence of trigonometric functions and obtain

$$q(\tau) := \sup_{-1 \leq c \leq 1} |1 - \tau(1 - c)|.$$

By definition, the supremum is smallest upper bound, i.e., the smallest λ such that

$$\forall_{-1 \leq c \leq 1} -\lambda \leq 1 - \tau(1 - c) \leq \lambda. \quad (8)$$

To determine the smallest λ satisfying (8), we have to eliminate the quantifiers, i.e. to solve a quantifier elimination problem.

A quantifier elimination problem is the problem to find a quantifier free formula that is equivalent to a quantified formula:

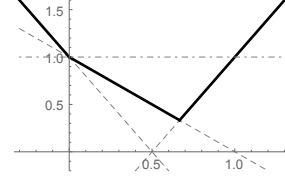


Fig. 2. Reduction of the high frequency modes as function of τ

Quantified formula:

$(Q_1)_{x_1} \dots (Q_n)_{x_n} A(x_1, \dots, x_n, y_1, \dots, y_m)$,
where $Q_i \in \{\exists, \forall\}$ and A is a finite boolean combination of polynomial inequalities

\Leftrightarrow

Quantifier free formula: $B(y_1, \dots, y_m)$,

where B is a finite boolean combination of polynomial inequalities.

The solution of such a problem is possible using CAD, cf. [4], [9]. By applying a CAD algorithm to (8), we obtain

$$\begin{aligned} &(\tau \leq 0 \wedge \lambda \geq 1 - 2\tau) \vee (0 < \tau \leq 1 \wedge \lambda \geq 1) \\ &\vee (\tau > 1 \wedge \lambda \geq -1 + 2\tau) \end{aligned} \quad (9)$$

Here, the smallest λ satisfying (9) is piecewise given by the terms $1 - 2\tau$, 1 and $-1 + 2\tau$. So, we obtain

$$q(\tau) = \begin{cases} 1 - 2\tau & \text{for } \tau \leq 0 \\ 1 & \text{for } 0 < \tau \leq 1 \\ -1 + 2\tau & \text{for } 1 < \tau. \end{cases}$$

We observe that there is no choice of τ such that $q(\tau) < 1$. This reflects knowledge on the Jacobi iteration (which is also true for other simple linear iteration schemes): the convergence is not robust in the grid size h_k , so the convergence rate cannot be bounded away from 1. (Although, we did not have an explicit dependence on the grid size h_k , the fact that we have considered an unbounded domain Ω is equivalent to considering an infinitely small grid size.)

It is known by intuition that simple linear iteration schemes reduce high frequency error modes. This statement can be formally expressed using LFA: Here, we only consider $\theta \in [0, \pi/2) \cup [3\pi/2, \pi)$ or, equivalently, $0 \leq c \leq 1$. In this case, we obtain using the same arguments as above

$$q_{SM}(\tau) = \sup_{0 \leq c \leq 1} |1 - \tau(1 - c)|$$

Again, we can compute using CAD (or still per hand) that

$$q_{SM}(\tau) = \begin{cases} 1 - 2\tau & \text{for } \tau \leq 0 \\ 1 - \tau & \text{for } 0 < \tau \leq \frac{2}{3} \\ -1 + 2\tau & \text{for } \frac{2}{3} < \tau. \end{cases}$$

This function is visualized in Fig. 2. We see that q_{SM} takes its minimal value $\frac{1}{3}$ for $\tau = \frac{2}{3}$.

III. ANALYSIS OF A MULTIGRID SOLVER

In the last section, we have seen that the Jacobi iteration reduces the high frequency error modes. The idea of a multigrid method is to use the fact that low frequency error modes can be resolved well also on a coarse grid. So, we combine the Jacobi iteration (or any other simple linear iteration scheme) with a coarse grid correction, which reduces the low frequency error modes.

We assume to have for $k = 1, 2, 3, \dots$ a hierarchy of grid levels, where a grid level k is obtained from grid level $k - 1$ by uniform refinement, i.e., in the case of one dimension: by subdividing each interval into two equally sized intervals. Starting from an iterate $\underline{x}_k^{(m)}$, the next iterate $\underline{x}_k^{(m+1)}$ of the multigrid method on grid level k is given by the following three steps:

- *Pre-Smoothing*: Compute

$$\underline{u}_k^{(m,1)} := \underline{u}_k^{(m)} + \tau(\text{diag } K_k)^{-1} \left(\underline{f}_k - K_k \underline{u}_k^{(m)} \right).$$

- *Coarse-grid correction*:

- Compute the defect $\underline{f}_k - K_k \underline{u}_k^{(m,1)}$ and restrict it to grid level $k - 1$:

$$\underline{r}_{k-1}^{(m)} := P_{k-1}^T \left(\underline{f}_k - K_k \underline{u}_k^{(m,1)} \right).$$

- Solve the following coarse-grid problem approximately:

$$K_{k-1} \underline{p}_{k-1}^{(m)} = \underline{r}_{k-1}^{(m)}. \quad (10)$$

- Prolongate $\underline{p}_{k-1}^{(m)}$ to the grid level k and add the result to the previous iterate:

$$\underline{u}_k^{(m,2)} := \underline{u}_k^{(m,1)} + P_{k-1} \underline{p}_{k-1}^{(m)}.$$

- *Post-Smoothing*: Compute

$$\underline{u}_k^{(m+1)} := \underline{u}_k^{(m,2)} + \tau(\text{diag } K_k)^{-1} \left(\underline{f}_k - K_k \underline{u}_k^{(m,2)} \right).$$

As we have nested spaces, i.e., $V_{k-1} \subseteq V_k$, there is canonical embedding from V_{k-1} into V_k , which is chosen as prolongation operator P_{k-1} .

If the problem (10) is solved exactly, we obtain the two-grid method. In practice, the problem (10) is approximately solved by applying one step (V-cycle) or two steps (W-cycle) of the multigrid method, recursively. Only on the coarsest grid level, (10) is solved exactly.

For computing the convergence rate of the multigrid solver, we set up again the iteration matrix \mathcal{G}_k , which is the product of the iteration matrix \mathcal{S}_k of the damped Jacobi iteration, of the iteration matrix \mathcal{C}_k of the coarse-grid correction and, once more, of the iteration matrix \mathcal{S}_k of the damped Jacobi iteration:

$$\mathcal{G}_k = \mathcal{S}_k \mathcal{C}_k \mathcal{S}_k,$$

where

$$\mathcal{C}_k = I - P_{k-1} K_{k-1}^{-1} P_{k-1}^T K_k$$

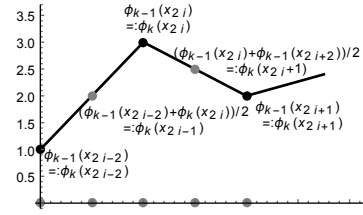


Fig. 3. Canonical embedding of V_{k-1} into V_k

and, as in the last section,

$$\mathcal{S}_k = I - \tau(\text{diag } K_k)^{-1} K_k.$$

As in the last section, we are interested in computing

$$q(\tau) = \|\mathcal{G}_k\|_{K_k} = \rho(\mathcal{G}_k).$$

To be able to determine the symbol of the iteration matrix \mathcal{G}_k , we have to take a closer look onto the prolongation operator P_{k-1} first. We recall that there is an isomorphism between \mathbb{R}^N , the space of coefficient vectors, and the function space V_k . So, for each coefficient vector $\underline{\phi}_k(\theta) = (\phi_{k,j}(\theta))_{j \in \mathbb{Z}}$, there is a function $\phi_k(\theta, \cdot) \in V_k$, which is assigned to it:

$$\phi_k(\theta, x) = \sum_{j \in \mathbb{Z}} \phi_{k,j}(\theta) \varphi_{k,j}(x).$$

By definition, P_{k-1} is the canonical embedding operator, which is visualized in Fig. 3.

The next step is to represent the function $\phi_{k-1}(2\theta, x)$ as a linear combination of functions on the fine grid. We observe, that this can be done using the ansatz

$$\phi_{k-1}(2\theta, x) = A\phi_k(\theta, x) + B\phi_k(\theta + \pi, x).$$

It is sufficient to consider the nodes $x_j = jh_k$ only. First we consider the even nodes x_{2j} , which are also nodes of the coarse grid:

$$\phi_{k-1}(2\theta, x_{2j}) = A\phi_k(\theta, x_{2j}) + B\phi_k(\theta + \pi, x_{2j}). \quad (11)$$

As the $(\varphi_{k,i})_{i \in \mathbb{Z}}$, form a nodal basis, (11) is equivalent to

$$\phi_{k-1,j}(2\theta) = A\phi_{k,2j}(\theta) + B\phi_{k,2j}(\theta + \pi),$$

$$e^{j2\theta i} = Ae^{2j\theta i} + Be^{2j(\theta + \pi)i}$$

and, finally,

$$1 = A + B.$$

Now, we consider the odd nodes x_{2j+1} , which do not occur on the coarse grid:

$$\phi_{k-1}(2\theta, x_{2j+1}) = A\phi_k(\theta, x_{2j+1}) + B\phi_k(\theta + \pi, x_{2j+1}). \quad (12)$$

As the $(\varphi_{k,i})_{i \in \mathbb{Z}}$, form a nodal basis, (12) is equivalent to

$$\begin{aligned} \frac{1}{2} (\phi_{k-1,j}(2\theta) + \phi_{k-1,j+1}(2\theta)) \\ = A\phi_{k,2j+1}(\theta) + B\phi_{k,2j+1}(\theta + \pi) \end{aligned}$$

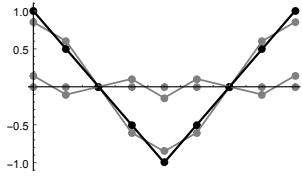


Fig. 4. Coarse-grid function $\phi_{k-1}(2\theta, x)$ in black and the two components $\frac{1}{2}(1 + \cos(\theta))\phi_k(\theta, x)$ and $\frac{1}{2}(1 - \cos(\theta))\phi_k(\theta + \pi, x)$ in gray.

and

$$\frac{1}{2} \left(e^{j2\theta i} + e^{2(j+1)\theta i} \right) = A e^{(2j+1)\theta i} + B e^{(2j+1)(\theta+\pi)i}$$

and, finally,

$$\underbrace{\frac{1}{2} \left(e^{-\theta i} + e^{\theta i} \right)}_{\cos(\theta)=} = A - B.$$

We obtain $A = \frac{1}{2}(1 + \cos(\theta))$ and $B = \frac{1}{2}(1 - \cos(\theta))$, which can be observed also in Fig. 4. This allows to introduce the symbol of the prolongation operator:

$$\widehat{P}_{k-1}(\theta) = \frac{1}{2} \begin{pmatrix} 1 + \cos(\theta) \\ 1 - \cos(\theta) \end{pmatrix}.$$

Here, the symbol cannot be understood as eigenvalue anymore. However, for all $\theta = [0, 2\pi)$, the prolongation operator P_{k-1} maps the linear span, spanned by

$$\underline{\phi}_{k-1}(2\theta) \quad (13)$$

to the linear span, spanned by

$$\underline{\phi}_k(\theta) \quad \text{and} \quad \underline{\phi}_k(\theta + \pi), \quad (14)$$

and the restriction operator P_{k-1}^T maps the linear span, spanned by (14), to the linear span, spanned by (13).

Having this, we can set up the symbol for the two-grid operator \mathcal{G}_k . We make use of the fact that the multiplication of \mathcal{G}_k with a vector in the linear span, given by the basis (14), maps into the same linear span. So, we have to set up the symbol of \mathcal{G}_k with respect to the two dimensional basis (14).

The symbol of S_k has been a scalar in the last section. This means that every frequency was preserved by the action of S_k . If we represent the symbol of S_k with respect to the basis (14), we just obtain a diagonal symbol:

$$\widehat{S}_k(\theta) = \begin{pmatrix} \widehat{S}_k(\theta) & \\ & \widehat{S}_k(\theta + \pi) \end{pmatrix},$$

where $\widehat{S}_k(\theta)$ is as defined in (7). Exactly the same way, we obtain the symbol $\widehat{\mathcal{K}}_k(\theta)$ based on $\widehat{K}_k(\theta)$, given in (6). Using this, we can determine the symbol of \mathcal{C}_k ,

$$\widehat{\mathcal{C}}_k(\theta) = I - \widehat{P}_{k-1}(\theta) [\widehat{K}_{k-1}(\theta)]^{-1} \widehat{P}_{k-1}(\theta)^* \widehat{\mathcal{K}}_k(\theta),$$

where A^* is the conjugate complex of A^T . Consequently, the symbol of \mathcal{G}_k is

$$\widehat{\mathcal{G}}_k(\theta) = \widehat{S}_k(\theta) \widehat{\mathcal{C}}_k(\theta) \widehat{S}_k(\theta).$$

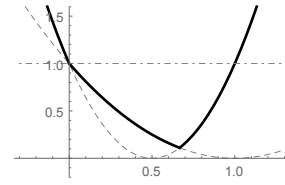


Fig. 5. Convergence rate of the multigrid solver as a function of τ

Here, the computation of $\widehat{\mathcal{G}}_k(\theta)$ and of $\rho(\widehat{\mathcal{G}}_k(\theta))$ is straightforward. We obtain:

$$\rho(\widehat{\mathcal{G}}_k(\theta)) = |(\tau - 1)^2 + \tau(3\tau - 2) \cos^2(\theta)|.$$

As in the last section, we are again interested in computing the supremum

$$q(\tau) = \rho(\mathcal{G}_k) = \sup_{\theta \in [0, 2\pi)} |(\tau - 1)^2 + \tau(3\tau - 2) \cos^2(\theta)|,$$

where we again substitute $\cos \theta$ by c and obtain

$$q(\tau) = \sup_{c \in [-1, 1]} |(\tau - 1)^2 + \tau(3\tau - 2)c^2|.$$

Also here, we can resolve the supremum using a CAD algorithm (or, still, per hand) and obtain

$$q(\tau) = \begin{cases} 1 - 4\tau + 4\tau^2 & \text{for } \tau < 0 \\ 1 - 2\tau + \tau^2 & \text{for } 0 \leq \tau < \frac{2}{3} \\ 1 - 4\tau + 4\tau^2 & \text{for } \frac{2}{3} \leq \tau. \end{cases}$$

This function is shown in Fig. 5. We see that q takes its minimal value $\frac{1}{9}$ for $\tau = \frac{2}{3}$.

So far, all computations had been so easy such that it would have been possible to do them per hand. However, the methodology presented in this section can be carried over to more complex (and more interesting) problems. The first extension would be to consider two or more dimensions. Here, one could represent everything use a tensor-product structure, cf. [10]. Consequently, one has to deal with tuples of d frequencies for d dimensional spaces. Also in this case, the θ_i can be substituted by $c_i := \cos(\theta_i)$ and solved as discussed in this session. However, the complexity of the expressions (particularly in terms of the polynomial degree) grows very fast if d is increased.

Besides that, the presented methodology can be extended to non-standard problems. This is of practical use because the convergence analysis has to be worked out for each problem class, separately. Here, LFA can be of great help.

One example where the presented approach has been applied in this fashion was in a in a joint work with V. Pillwein¹, cf. [7], [8], where LFA and CAD have been used to compute convergence rates of a multigrid solver for a *system of PDEs* which characterizes the solution of an optimal control problem. There, not only the robustness of the convergence rates in the grid size h_k , but also the robustness of the convergence rates in a regularization parameter, which is part of the

¹Research Institute for Symbolic Computation, Johannes Kepler University Linz, Austria

problem description, was of interest and could be studied. The supplementary material, that came with the cited paper, is available in the web². The author wants to refer the reader, which is interested in analyzing multigrid convergence, to that material.

In the following of the present paper, the author wants to draw the reader's attention to another application of LFA that is also of interest in numerical analysis: the estimation of approximation error estimates.

IV. ESTIMATE THE APPROXIMATION ERROR

In this section, we are interested in comparing estimates of the approximation error

$$\inf_{u_k \in V_k} \|u - u_k\|_{L^2(\Omega)}$$

for different kinds of discretizations. One of the discretizations will be the Courant element, two more will be introduced below. Here and in what follows $\|\cdot\|_{L^2(\Omega)}$ is the standard L^2 -norm, i.e., $\|f\|_{L^2(\Omega)}^2 := \int_{\Omega} f^2(x) dx$

One important approximation error estimate reads as follows:

$$\inf_{u_k \in V_k} \|u - u_k\|_{L^2(\Omega)}^2 \leq C_A h_k^2 |u|_{H^1(\Omega)}^2$$

for all $u \in L^2(\Omega)$, where $C_A > 0$ is a constant, h_k is the grid size and $|u|_{H^1(\Omega)} := \|u'\|_{L^2(\Omega)}$. For classical discretizations, it is well-known that such an estimate exists. However, often there is no realistic bound for the constant C_A . So, it might be of interest to compute an realistic (not necessarily sharp) upper bound for the constant C_A for discretizations of interest.

The approximation error can be bounded from above using an interpolation error $\|u - \Pi_k u\|_{L^2(\Omega)}$, where $\Pi_k : H^1(\Omega) \rightarrow V_k$ is an arbitrarily projection operator. So, it suffices to estimate

$$\|u - \Pi_k u\|_{L^2(\Omega)}^2 \leq C_A h_k^2 |u|_{H^1(\Omega)}^2 \quad (15)$$

for any projection operator Π_k . Using the following lemma, we show (15) for Π_k being the H^1 -orthogonal projection.

Lemma 1: Let for all grid levels $k \in \mathbb{N}$, the operator Π_k be the H^1 -orthogonal projection from $H^1(\Omega)$ into V_k . Assume that for all k the following *quantitative* estimate on two consecutive grids is satisfied:

$$\|(I - \Pi_k)u_{k+1}\|_{L^2(\Omega)}^2 \leq C_A h_k^2 |u_{k+1}|_{H^1(\Omega)}^2 \quad (16)$$

for all $u_{k+1} \in V_{k+1}$. Moreover, we assume to know *qualitatively* that

$$\|(I - \Pi_k)u\|_{L^2(\Omega)} \rightarrow 0 \text{ for } k \rightarrow \infty \quad (17)$$

for all $u \in L^2(\Omega)$. Then the following estimate is satisfied:

$$\|(I - \Pi_k)u\|_{L^2(\Omega)}^2 \leq 4C_A h_k^2 |u|_{H^1(\Omega)}^2$$

for all $u \in L^2(\Omega)$.

Proof: The proof is based on a simple telescoping argument. Due to (17), for any $\epsilon > 0$ there is some $K > 0$ such that $\|(I - \Pi_K)u\|_{L^2(\Omega)} < \epsilon |u|_{H^1(\Omega)}$. Now, we obtain due to the

triangular inequality, (16) and the fact that the H^1 -orthogonal projection is stable in $H^1(\Omega)$, i.e., $|\Pi_k u|_{H^1(\Omega)} \leq |u|_{H^1(\Omega)}$,

$$\begin{aligned} & \|(I - \Pi_k)u\|_{L^2(\Omega)} \\ & \leq \|(I - \Pi_K)u\|_{L^2(\Omega)} + \sum_{m=k}^{K-1} \|(I - \Pi_m)\Pi_{m+1}u\|_{L^2(\Omega)} \\ & \leq \left(\epsilon + \sum_{m=k}^{K-1} C_A^{1/2} h_m \right) |u|_{H^1(\Omega)} =: \Psi. \end{aligned}$$

As $h_m = 2^{k-m} h_k$, we obtain using the summation formula for the geometric series that $\Psi \leq (\epsilon + 2C_A^{1/2} h_k) |u|_{H^1(\Omega)}$ and for $\epsilon \rightarrow 0$ the desired result. ■

The statement (17) is well-known for all standard discretizations. However, there might not be a good estimate for C_A . So, we are interested in the results by this lemma. The estimate (16) can be treated using LFA. We can rewrite (16) in matrix-vector notation as follows:

$$\|(I - P_k K_k^{-1} P_k^T K_{k+1}) \underline{u}_{k+1}\|_{M_{k+1}}^2 \leq C_A h_k^2 \|\underline{u}_{k+1}\|_{K_{k+1}}^2,$$

where $M_k := (m_{i,j})_{i,j=1}^N := (\int_{\Omega} \varphi_{k,i}(x) \varphi_{k,j}(x) dx)_{i,j=1}^N$ is the mass matrix. Here, the upper bound is obtained using the matrix norm:

$$C_A^{1/2} = \frac{1}{h_k} \left\| M_{k+1}^{1/2} (I - P_k K_k^{-1} P_k^T K_{k+1}) K_{k+1}^{-1/2} \right\|.$$

Using the definition of the Euclidean norm and the fact that $(I - P_k K_k^{-1} P_k^T K_{k+1})^2 = (I - P_k K_k^{-1} P_k^T K_{k+1})$, we obtain

$$C_A = \frac{1}{h_k^2} \rho \left(\underbrace{M_{k+1} (I - P_k K_k^{-1} P_k^T K_{k+1}) K_{k+1}^{-1}}_{\mathcal{G}_{k+1} :=} \right).$$

Here, again, the spectral radius can be determined using the symbol

$$C_A = \sup_{\theta \in [0, 2\pi)} \rho \left(\widehat{\mathcal{G}}_{k+1}(\theta) \right), \text{ where}$$

$$\widehat{\mathcal{G}}_{k+1}(\theta) := \frac{1}{h_k^2} \widehat{\mathcal{M}}_{k+1}(\theta) \widehat{\mathcal{C}}_{k+1}(\theta) \left(\widehat{\mathcal{K}}_{k+1}(\theta) \right)^{-1},$$

$$\widehat{\mathcal{C}}_{k+1}(\theta) := \left(I - \widehat{P}_k(\theta) \left(\widehat{K}_k(\theta) \right)^{-1} \widehat{P}_k(\theta)^* \widehat{\mathcal{K}}_{k+1}(\theta) \right).$$

As we have mentioned above, we are interested in computing C_A for different discretizations. The details can be found in an accompanying Mathematica notebook, which is available in the web³, the main ideas will be given in the following three subsections.

A. The Courant element

The symbols $\widehat{\mathcal{K}}_{k+1}(\theta)$ and $\widehat{P}_k(\theta)$ for the Courant element have already been determined in the last section. The mass matrix M_k has also a tridiagonal form. The symbol can be computed completely analogous as for the stiffness matrix:

$$\widehat{\mathcal{M}}_{k+1}(\theta) = \begin{pmatrix} \widehat{M}_{k+1}(\theta) & \\ & \widehat{M}_{k+1}(\theta + \pi) \end{pmatrix},$$

²<http://www.risc.jku.at/people/vpillwei/sLFA/>

³<http://www.numa.uni-linz.ac.at/~stefant/J3362/slfa/>

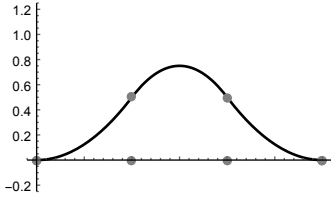


Fig. 6. Basis functions for the P^2 -spline discretization

where

$$\widehat{M}_{k+1}(\theta) = \frac{1}{6}(e^{-\theta i} + 4 + e^{\theta i}).$$

Based on this, we can derive

$$\widehat{\mathcal{G}}_{k+1}(\theta) = \frac{1}{12} \begin{pmatrix} 2 + \cos \theta & -2 + \cos \theta \\ -2 - \cos \theta & 2 - \cos \theta \end{pmatrix}.$$

The eigenvalues of $\widehat{\mathcal{G}}_{k+1}(\theta)$ are 0 and $\frac{1}{3}$. As this is already independent of θ , we immediately obtain that for the Courant element $C_A = \frac{1}{3}$ is satisfied.

B. A P^2 -spline discretization

We can set up the same framework also for other discretizations, like the discretization with splines. Here, assume that V_k is the space of all continuously differentiable functions, which are piecewise polynomials of degree 2. One possible basis for V_k is the basis of B-splines:

$$\varphi_{k,i}(x) = \begin{cases} \frac{1}{2h_k^2}(x - x_{i-1})^2 & \text{for } x_{i-1} \leq x < x_i \\ \frac{3}{4} - \frac{1}{4h_k^2}(2x - x_i - x_{i+1})^2 & \text{for } x_i \leq x < x_{i+1} \\ \frac{1}{2h_k^2}(x - x_{i+2})^2 & \text{for } x_{i+1} \leq x < x_{i+2} \\ 0 & \text{otherwise,} \end{cases}$$

where $x_i = ih_k$, see Fig. 6 for a visualization of such a basis function.

For the B-splines, we can again compute the integrals that are necessary to set up the mass matrix M_k . As the support of the B-splines is larger than the support of the basis functions of the Courant element, we obtain a band matrix with a bandwidth of 5, with $m_{i,i} = \frac{66}{120}h_k$, $m_{i,i\pm 1} = \frac{26}{120}h_k$ and $m_{i,i\pm 2} = \frac{1}{120}h_k$. Also for this case, we can determine the symbol

$$\widehat{M}_k(\theta) = \frac{h_k}{120} (e^{-2i\theta} + 26e^{-i\theta} + 66 + 26e^{i\theta} + e^{2i\theta}).$$

We can set up the the stiffness matrix K_k and its symbol in a completely analogous way and obtain

$$\widehat{K}_k(\theta) = \frac{1}{6h_k} (-e^{-2i\theta} - 2e^{-i\theta} + 6 - 2e^{i\theta} - e^{2i\theta}).$$

For setting up the symbol of the prolongation operator P_{k-1} , it is sufficient to solve again the equations (11) and (12). For details, we refer to the Mathematica notebook. The overall symbol $\widehat{\mathcal{G}}_{k+1}(\theta)$ is again just obtained by multiplying the individual symbols. The eigenvalues of $\widehat{\mathcal{G}}_{k+1}(\theta)$ are 0 and

$$\frac{-51 + 14 \cos(2\theta) + \cos(4\theta)}{40(-2 + \cos(\theta))(2 + \cos(\theta))(2 + \cos(2\theta))}. \quad (18)$$

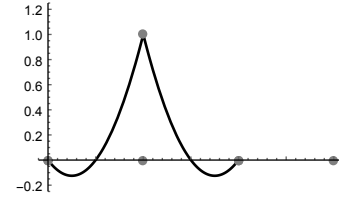


Fig. 7. Basis functions of the first kind of the P^2 -discretization

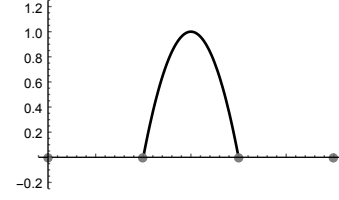


Fig. 8. Basis functions of the second kind of the P^2 -discretization

This second eigenvalue can be rewritten using the replacement $\cos \theta \rightarrow c$ as rational function, where the terms $\cos(2\theta)$ and $\cos(4\theta)$ are treated using the corresponding Chebyshev polynomials. Here we obtain – using CAD – that $\frac{2}{5}$ is the largest value taken by (18), so we obtain $C_A = \frac{2}{5}$.

C. A standard P^2 -discretization

Besides the spline functions, there is another possibility of setting up a discretization based on polynomials of degree 2, which is even more popular in finite elements: we define V_k to be the space of continuous functions that are piecewise polynomials of degree 2. Here, we can introduce a nodal basis, i.e., a basis where each basis function is associated to node (this basis function takes the value 1 on that node and the value 0 on all other nodes). Here, the nodes are allocated on the ends of the intervals (as for the Courant element) and, additionally, on the midpoints of the elements. Here, we have two types of basis functions, cf. Fig. 7 and Fig. 8 for visualizations.

Because there are two types of elements, the mass matrix has alternating coefficients, see the Mathematica notebook for details:

$$M_k = \frac{h_k}{30} \begin{pmatrix} \ddots & \ddots & \ddots & \ddots & \ddots & \ddots & \ddots & \ddots & \ddots \\ \ddots & 8 & 2 & -1 & & & & & \\ \ddots & 2 & 16 & 2 & 0 & & & & \\ \ddots & -1 & 2 & 8 & 2 & -1 & & & \\ & & 0 & 2 & 16 & 2 & 0 & & \\ & & & -1 & 2 & 8 & 2 & \ddots & \\ & & & & 0 & 2 & 16 & \ddots & \\ & & & & & \ddots & \ddots & \ddots & \ddots \end{pmatrix}.$$

For determining the symbol of M_k , we rewrite M_k as a sum of a band-matrix and of a residual matrix with alternating signs:

$$M_k = A_k + B_k,$$

where $A_k = (a_{i,j})_{i,j \in \mathbb{Z}}$ is a band matrix with $a_{i,i} = \frac{2}{5}h_k$, $a_{i,i\pm 1} = \frac{1}{15}h_k$ and $a_{i,i\pm 2} = -\frac{1}{60}h_k$ and B_k is a matrix with

alternating coefficients:

$$B_k := \frac{h_k}{60} \begin{pmatrix} \ddots & \ddots & \ddots & \ddots & \ddots & \ddots & \ddots \\ \ddots & -8 & 0 & -1 & & & \\ \ddots & 0 & 8 & 0 & 1 & & \\ & -1 & 0 & -8 & 0 & -1 & \\ & & 1 & 0 & 8 & 0 & \ddots \\ & & & -1 & 0 & -8 & \ddots \\ & & & & \ddots & \ddots & \ddots \end{pmatrix}.$$

Based on this decomposition, we can find the symbol. The symbol of A_k is obviously just

$$\widehat{A}_k(\theta) = \frac{h_k}{60} (-e^{-2\theta i} + 4e^{-\theta i} + 24 + 4e^{\theta i} - e^{2\theta i}).$$

The symbol corresponding to B_k is determined as follows:

$$\begin{aligned} B_k \underline{\phi}_k(\theta) &= (2(-1)^j e^{j\theta i} + (-1)^j (e^{(j+2)\theta i} + e^{(j-2)\theta i}))_{j \in \mathbb{Z}} \\ &= (2e^{j(\theta+\pi)i} + (e^{2\theta i} + e^{-2\theta i})e^{j(\theta+\pi)i})_{j \in \mathbb{Z}} \\ &= \underbrace{(2 + e^{2\theta i} + e^{-2\theta i})}_{\widehat{B}_k(\theta) :=} \underline{\phi}_k(\theta + \pi). \end{aligned}$$

So, we obtain

$$M_k \underline{\phi}_k(\theta) = \widehat{A}_k(\theta) \underline{\phi}_k(\theta) + \widehat{B}_k(\theta) \underline{\phi}_k(\theta + \pi)$$

and, as $\theta + 2\pi \approx \theta$, also

$$M_k \underline{\phi}_k(\theta + \pi) = \widehat{B}_k(\theta + \pi) \underline{\phi}_k(\theta) + \widehat{A}_k(\theta + \pi) \underline{\phi}_k(\theta + \pi).$$

This shows, that M_k does not preserve a one dimensional linear span anymore, but a two-dimensional span, spanned by $\underline{\phi}_k(\theta)$ and $\underline{\phi}_k(\theta + \pi)$. This is similar to the coarse-grid operator in the last section and in the last two subsections. So, the symbol is a representation of M_k with respect to the basis formed by these two vectors:

$$\widehat{M}_k(\theta) = \begin{pmatrix} \widehat{A}_k(\theta) & \widehat{B}_k(\theta) \\ \widehat{B}_k(\theta + \pi) & \widehat{A}_k(\theta + \pi) \end{pmatrix}.$$

The symbol $\widehat{K}_k(\theta)$ of the stiffness matrix K_k can be determined completely analogous.

Also the symbol of the prolongation operator can be determined similarly to the cases of the last sections. However, we need four frequencies to be able to reconstruct a function on the coarse grid, so we use the ansatz $\phi_{k-1}(2\theta, x) = \sum_{j=0}^3 A_j \phi_k(\theta + j\pi/2, x)$, where it is again sufficient to consider the values on the nodes (midpoints and end points of the intervals). This can be used to determine the coefficients A_0, A_1, A_2 and A_3 .

For all $\theta = [0, 2\pi)$, the prolongation operator P_{k-1} maps the linear span, spanned by

$$\underline{\phi}_{k-1}(2\theta) \quad \text{and} \quad \underline{\phi}_{k-1}(2\theta + \pi) \quad (19)$$

to the linear span, spanned by

$$\underline{\phi}_k(\theta), \quad \underline{\phi}_k(\theta + \pi/2), \quad \underline{\phi}_k(\theta + \pi) \quad \text{and} \quad \underline{\phi}_k(\theta + 3\pi/2), \quad (20)$$

and the restriction operator P_{k-1}^T maps the linear span, spanned by (20), to the linear span, spanned by (19). So, the

symbol \widehat{P}_{k-1} is a 2×4 -matrix, for details we refer to the Mathematica notebook. Based on the symbols of the individual components, we can again compute $\widehat{\mathcal{G}}_{k+1}(\theta)$, the symbol of the overall operator. The eigenvalues of this matrix are $0, 0, \frac{1}{30}$ and $\frac{1}{10}$, so we obtain $C_A = \frac{1}{10}$.

So, we have seen that the constant C_A takes the value $\frac{1}{3}$ for the Courant element, the value $\frac{2}{5}$ for the P^2 -spline discretization and $\frac{1}{10}$ for the standard P^2 discretization.

This indicates that the standard P^2 discretization has the best approximation properties. However, the standard P^2 discretization needs two degrees of freedom per element, while the other two discretizations need, each, one degree of freedom per element. By defining \hat{h}_k to be the distance between two nodes, i.e., $\hat{h}_k = \frac{1}{2}h_k$ for the standard P^2 -discretization and $\hat{h}_k = h_k$ for the other two discretizations, we can redefine the approximation error estimate as follows:

$$\|u - \Pi_k u\|_{L^2(\Omega)}^2 \leq \hat{C}_A \hat{h}_k^2 |u|_{H^1(\Omega)}^2.$$

Here, we obtain $\hat{C}_A = \frac{1}{3}$ for the Courant element and $\hat{C}_A = \frac{2}{5}$ for both of the quadratic discretizations.

As we have already mentioned, an extension to two dimensions is possible, however the terms get much more complicated. We refer to the complementary material, where we made an attempt to generalize the analysis to two dimensions.

V. CONCLUDING REMARKS

We have seen that the terms that are constructed using LFA can be treated well using symbolic computation, particularly using CAD. Moreover, we have seen that the method of LFA can be applied in a wide range of problems. Besides its application to multigrid solvers, which is well studied in literature, cf. [1], [2], [10], LFA can be applied to other problems occurring in numerical analysis, like the computation of approximation error estimates.

REFERENCES

- [1] A. Brandt, *Multi-level adaptive solutions to boundary-value problems*, Math. Comp. **31** (1977), 333 – 390.
- [2] ———, *Rigorous Quantitative Analysis of Multigrid, I: Constant Coefficients Two-Level Cycle with L_2 -Norm*, SIAM J. on Numerical Analysis **31** (1994), no. 6, 1695 – 1730.
- [3] S. Brenner and L. Scott, *The Mathematical Theory of Finite Element Methods*, Springer-Verlag, New York, 1994.
- [4] G.E. Collins, *Quantifier elimination for real closed fields by cylindrical algebraic decomposition*, Automata theory and formal languages (Second GI Conf., Kaiserslautern, 1975), Springer, Berlin, 1975, pp. 134 – 183. Lecture Notes in Comput. Sci., Vol. 33.
- [5] W. Hackbusch, *Multi-Grid Methods and Applications*, Springer, Berlin, 1985.
- [6] H. Hong, R. Liska, and S. Steinberg, *Applications of quantifier elimination (Albuquerque, NM, 1995)*, J. Symbolic Comput. **24** (1997), no. 2, 161 – 187.
- [7] V. Pillwein and S. Takacs, *Smoothing analysis of an all-at-once multigrid approach for optimal control problems using symbolic computation*, Numerical and Symbolic Scientific Computing: Progress and Prospects (U. Langer and P. Paule, eds.), Springer, Wien, 2011.
- [8] ———, *An exemplary convergence analysis of a multigrid method using symbolic computation*, 2012, submitted.
- [9] A. Strzeboński, *Solving systems of strict polynomial inequalities*, J. Symbolic Comput. **29** (2000), no. 3, 471 – 480.
- [10] U. Trottenberg, C. Oosterlee, and A. Schüller, *Multigrid*, Academic Press, London, 2001.